Applied Thermal Engineering 91 (2015) 288–297

Contents lists available at ScienceDirect

Applied Thermal Engineering

journal homepage: www.elsevier.com/locate/apthermeng

Research paper

Enhanced pool-boiling heat transfer on laser-made hydrophobic/superhydrophilic polydimethylsiloxane-silica patterned surfaces

Matevž Zupančič [a,*], Miha Steinbücher [b], Peter Gregorčič [a], Iztok Golobič [a]

[a] University of Ljubljana, Faculty of Mechanical Engineering, Aškerčeva 6, 1000 Ljubljana, Slovenia
[b] Helios TBLUS d.o.o, Količevo 65, 1230 Domžale, Slovenia

HIGHLIGHTS

- Boiling heat transfer on polydimethylsiloxane-silica film is studied experimentally.
- Biphilic (138°/<1°) micropatterned surfaces are produced with pulsed Nd:YAG laser.
- Smaller hydrophobic spots reduce bubble diameter and increase nucleation frequency.
- The highest HTC is achieved on biphilic surface with the smallest hydrophobic spots.
- Uniform superhydrophilic surface exhibit 350% higher CHF compared to bare surface.

ARTICLE INFO

Article history:
Received 17 February 2015
Accepted 12 August 2015
Available online 21 August 2015

Keywords:
Pool boiling
Heat transfer enhancement
Biphilic micropattern
Laser-processed surface
High-speed IR thermography
Polydimethylsiloxane-silica coating

ABSTRACT

This study presents the application of hydrophobic polydimethylsiloxane-silica coating used for the development of biphilic surfaces that are designed to enhance the heat transfer during boiling. Surface analyses showed that this coating exhibits a high hydrophobicity due to its hierarchical structure and the use of hydrophobic polymer. An appropriate thermal treatment leads to the oxidation of the methyl groups and a formation of silicon oxide and silicon carbide that result in a wettability transition from hydrophobic to superhydrophilic. On this basis, we manufactured hydrophobic/superhydrophilic patterns on stainless-steel foils using a pulsed Nd:YAG laser. The uniform, superhydrophilic surface exhibited a 350% larger critical heat flux (CHF) than bare stainless-steel foil. High-speed IR thermography revealed that the increased wettability reduced the bubble contact diameter, allowed a higher density of active nucleation sites, and delayed the dry-out. The biphilic surfaces with differently sized hydrophobic spots exhibited the highest heat transfer coefficients, with an up to 200% higher CHF compared to the bare stainless steel. Smaller hydrophobic spots reduced the bubble diameter and increased the nucleation frequency. However, surfaces with larger hydrophobic regions promoted boiling incipience and exhibited higher heat transfer coefficients at low heat fluxes. These results suggest that the optimal biphilic pattern could only be determined for a particular operating point. Our data provide a new insight into the complex phenomena of nucleate pool boiling on chemically and mechanically heterogeneous surfaces.

© 2015 Elsevier Ltd. All rights reserved.

1. Introduction

Due to the large latent heat of the working fluids, boiling heat transfer is a very promising cooling method in the high-heat-flux applications, such as the cooling of nuclear-fuel claddings [1,2], integrated circuits [3,4], and concentrated photovoltaics [5]. The performance of boiling heat transfer is best characterized by the heat transfer coefficient (HTC) and the critical heat flux (CHF), which is the upper limit of the nucleate boiling regime. A desire to increase the HTC and the CHF has led to the development of many new techniques over the past few decades [6]. In pool boiling, these techniques are generally based on tailoring the surface and include combinations of micropores, nanopores and tunnels [7,8]; fins [9,10]; nanowires and nanotubes [4,11,12]; hydrophobic and

* Corresponding author. University of Ljubljana, Faculty of Mechanical Engineering, Laboratory for Thermal Technology, Aškerčeva 6, 1000 Ljubljana, Slovenia. Tel.: +386 1 4771 309.
E-mail address: matevz.zupancic@fs.uni-lj.si (M. Zupančič).

http://dx.doi.org/10.1016/j.applthermaleng.2015.08.026
1359-4311/© 2015 Elsevier Ltd. All rights reserved.

hydrophilic surfaces and patterns [13–16]; and the use of nanofluids as a working fluid [17].

The authors Tang et al. [18], for example, showed that during the saturated pool boiling of water on a nanoporous copper surface (50–200-nm pores), a reduction of 63% in the wall superheat and an increase of 173% in the HTC compared to the plain surface were achieved. Also, the onset of nucleate boiling was lowered by 5 K on the nanoporous surface. In a recent study by Dong et al. [19], the silicon surfaces were covered with lithographically made microfins with diameters ranging from 5 to 100 μm and heights from 5 to 50 μm. The CHF on the structured surfaces was 550–700 kW/m^2, compared to the plain surface, where the CHF was only 400 kW/m^2. The HTC was improved by at least 100% in all cases. The heat transfer enhancement on the structures with diameters of 50 and 100 μm was presumably due to the increased effective area of the heat transfer. On smaller structures, with the diameters of 5 and 10 μm, a higher nucleation frequency and an increased number of nucleation sites were reported to be the main reasons for the HTC and CHF enhancements.

In the past few years, hydrophobic and hydrophilic surface patterning have shown promising results when it comes to increasing the heat transfer performance during pool boiling. Coyle et al. [14] presented a method of developing hydrophobic (static contact angle $\theta = 135^\circ$) spots of different shapes with a 260-μm spot diameter and 1.5-mm pitch on a superhydrophilic ($\theta < 5^\circ$) surface. They found that the hydrophobic spots serve as preferential nucleation sites, even though the spot patterning did not greatly enhance the CHF, compared to the purely hydrophilic surface. Patterned and purely hydrophilic surfaces had a 50–90% enhancement in the CHF compared to the bare, uncoated surface, since the hydrophilic region increased the rewetting after the bubble nucleation and therefore delayed the dry-out. However, Betz, et al. [13] found that hydrophobic spots on a hydrophilic surface improved both the CHF and HTC over a plain hydrophilic surface by 65% and 100%, respectively. Betz et al. [15] later developed a superbiphilic surface on a silicon substrate where the contact angles of the water reached 0° and more than 150° on the superhydrophilic and superhydrophobic regions, respectively. The superhydrophobic spots were around 40 μm in diameter and had a pitch of 100 μm. According to their theory, the hydrophobic spots provide active nucleation sites and the size of the spot dictates the contact diameter of the evaporating bubble, which also affects the nucleation frequency. The highest CHF (1350 kW/m^2) was achieved on superhydrophilic surfaces and the highest HTC (over 150 kW/m^{2}K), on superbiphilic surfaces, where the superheat at the onset of the nucleate boiling was around 1 K. The superheat at the onset of the nucleate boiling on the superhydrophobic surface was reported to be only 0.1 K, which should in fact drastically improve the HTC. However, a vapor film covered the heated surface and reduced the HTC shortly after the onset of boiling, which was also the case in Ref. [20].

Therefore, the surfaces that provide an enhanced HTC and CHF during nucleate boiling offer at least one of the following improvements: (i) a higher density of the active nucleation sites; (ii) a higher nucleation frequency; (iii) a smaller bubble contact area; and (iv) a lower superheat at the onset of the nucleate boiling. Biphilic and superbiphilic surfaces show promising results, as the size and the number of hydrophobic (HPO) spots dictate the nucleation site density and the bubble diameter. On the other hand, the hydrophilic (HPI) region ensures "the suction" of the liquid towards the nucleation sites and prevents the bubbles' coalescence. Thus, the HPI region delays the formation of an overheated, dried-out area and, consequently, enhances the CHF. The mechanical resistance, the thermal stability, and the manufacturing costs are still the main drawbacks of biphilic surfaces [6], since fabrication often includes relatively challenging and costly techniques, such as photolithography, etching, sputtering and different sol–gel procedures. Further work is needed in order to develop durable, easy-to-make, and inexpensive biphilic surfaces and also to better understand the pool-boiling phenomena on the patterned hydrophobic/hydrophilic surfaces.

In this study we present the application of a hydrophobic coating based on polydimethylsiloxane (PDMS) resin and hydrophobic fumed silica that can be easily air-sprayed onto large surfaces. Since the coating can become superhydrophilic after a certain thermal treatment procedure, we created hydrophobic/superhydrophilic patterns on thin stainless-steel foils by using a Nd:YAG pulsed laser. Various analysis techniques were first used to characterize the surfaces and explain the wettability transition. Then we performed the saturated pool-boiling experiments where high-speed IR and video cameras were used to obtain a visualization of the departing bubbles with the corresponding local wall-temperature measurements. We have measured the local wall temperatures on the hydrophobic spots and the surrounding superhydrophilic region during boiling, with a frame rate of 1000 fps and a 250-μm resolution. Our data provide a new insight into the complex phenomena of nucleate pool boiling on chemically and mechanically heterogeneous surfaces.

2. Material and methods

2.1. Fabrication of the biphilic surface

The hydrophobic coating was fabricated as follows. The polydimethylsiloxane (PDMS) coated fumed silica with a specific surface area of 200 m^2/g and a primary particle size of approximately 10 nm was first dispersed in a PDMS resin solution in an organic solvent. The dispersion was then grinded in a vertical ball mill to a fineness of 0 μm, according to the ISO 1524. The mass ratio between the silica and the solid PDMS resin was 1:1. The so-prepared coating was air-sprayed onto the 25-μm-thick stainless-steel foils, which were used as the base for the heater surfaces. After the spraying, the foils were heat cured for 30 min at 230 °C in the air.

The basic PDMS-silica coating was highly hydrophobic, as shown in Fig. 1. In order to achieve the transition from hydrophobic to superhydrophilic we used a pulsed Nd:YAG laser with a spot size on the substrate of 50 μm. Experiments revealed that by our laser system the optimal results were achieved with a repetition frequency of 3 kHz and a pulse energy of 1.0 mJ. Using these parameters, the pulse duration was 340 ns. The laser had an integrated scanning system with a 2-μm resolution, which allowed us to create biphilic patterns. The scanning velocity was set to 150 mm/s. A

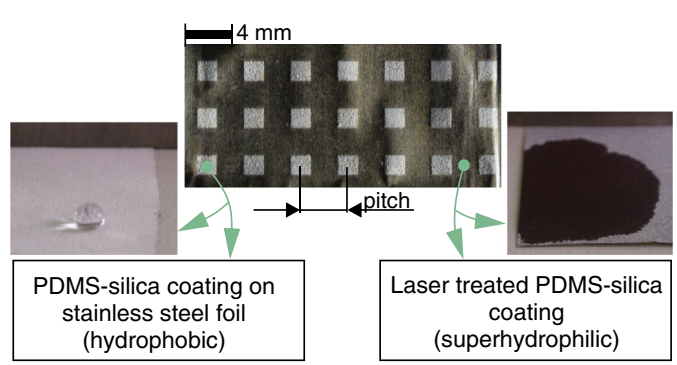

Fig. 1. Sample of a laser-made biphilic pattern on a stainless-steel foil. A drop of water on a hydrophobic PDMS-silica coating (the left-hand-side image) and a superhydrophilic coating (the right-hand-side image) after the laser treatment is shown.

Table 1
A detailed list of the equipment used for the manufacture and characterization of the developed surfaces.

Coating manufacturing	
Grinding	Dispermat vertical bead mill; diameter of zirconium grinding balls: 0.7 mm.
Air spraying	SATAjet paint air-spray gun; air pressure: 2 bar; nozzle diameter; 1.3 mm.
Heat curing	Laboratory furnace Kambič LSP-190; temperature accuracy: ±5 °C at T > 100 °C.
Laser treatment	Q-switched Nd:Yag laser Fotona YAG 22 CLASS MARK; $\lambda = 1064$ nm; spot size: 50 μm; scanning resolution: 2 μm.
Annealing	Nabertherm L 5/11 furnace with P320 controller.
Surface characterization	
Contact angles	Krüs DSA 100; measurement resolution: 0.1°; limit of measurement: 1°.
AFM microscopy	Park XE100; spatial resolution: 500 pm; background noise: 150 pm.
FTIR spectroscopy	Thermo Nicolet NEXUS.
SEM/EDS analysis	Jeol JSM T330A with Tracor Northern Z-Max 30 Series EDS system; spatial resolution: 5 nm.

typical example of a laser-made hydrophobic/superhydrophilic surface used in the experiments is shown in Fig. 1. A list of the equipment used for the manufacture and characterization of the surfaces is given in Table 1.

The pool-boiling experiments were conducted on six different surfaces, listed in Table 2. All the hydrophobic/superhydrophilic patterns were made with a laser and the uniform, superhydrophilic surface was made by annealing the PDMS-silica-coated foil for 8 h at 600 °C.

2.2. Experimental setup

The experimental setup for the saturated pool-boiling experiments on thin metal foils is schematically shown in Fig. 2. The pool-boiling chamber with external dimensions of 170 × 100 × 100 mm^3 was made of two steel plates and walls made of double-pane glass to enable visualization and at the same time to minimize the heat losses during the measurements, as the hot air was blown between the panes of glass. The heater unit (its cross-section is shown on the left-hand side of Fig. 2) was mounted on the bottom of the boiling chamber. It consisted of a stainless-steel foil (17 × 27 mm^2) and two copper electrical contacts, positioned on the ceramic base (MACOR), which had a rectangular borehole milled in the center to enable IR thermography. A golden mirror was placed at an angle of 45° under the chamber to allow the IR camera to safely record the temperature fields at the bottom of the thin foil.

Double-distilled water was used as the working fluid and was boiled for two hours prior to the experiments to remove most of the

Table 2
List of the surfaces used in the pool-boiling experiments.

Label	Description	Hydrophobic spot size, mm^2	Pitch, mm	Hydrophobic spot density, cm^{-2}
SS	25-μm-thick stainless-steel foil S316, Precision Brand	/	/	/
HPO_0	Polydimethylsiloxane-silica hydrophobic coating	/	/	/
$SHPI_0$	Annealed PDMS-silica coating	/	/	/
BPI_2	Biphilic surface; laser-treated HPO coating	2.0 × 2.0	4	6.3
BPI_1	Biphilic surface; laser-treated HPO coating	1.0 × 1.0	3	11.1
$BPI_{0.25}$	Biphilic surface; laser-treated HPO coating	0.25 × 0.25	1.5	44.4

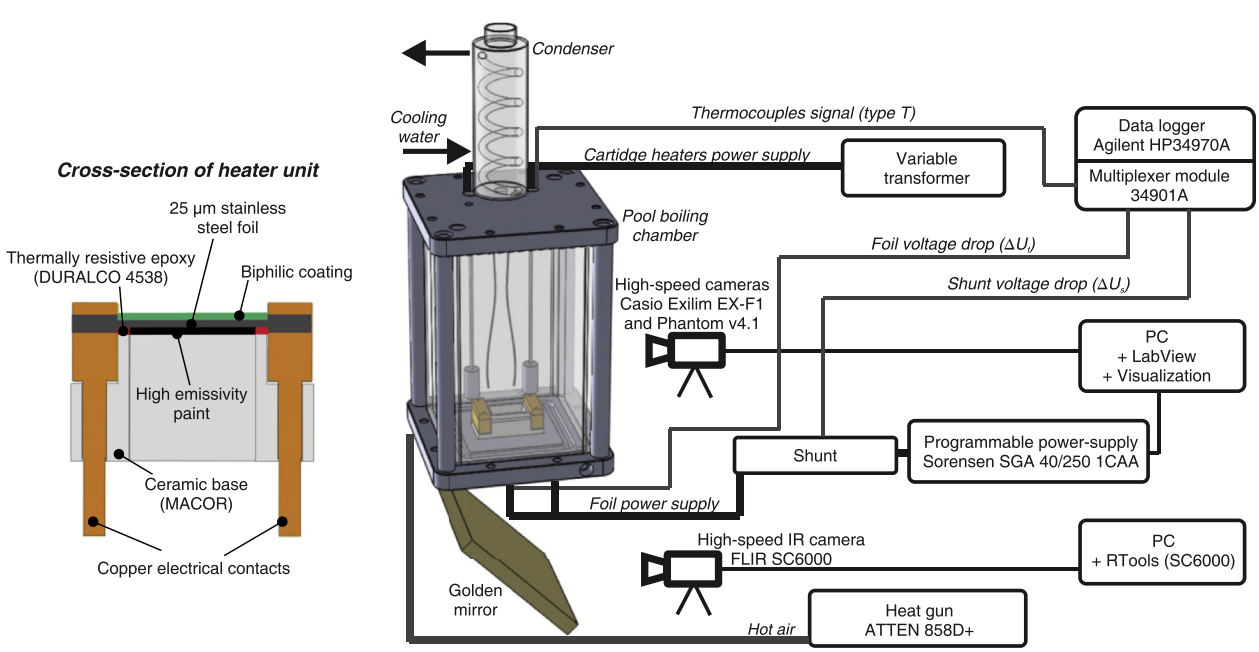

Fig. 2. Pool-boiling experimental setup and a cross-section view of the thin-metal-foil heater unit.

dissolved gases. Two immersed cartridge heaters were used for the preheating and to maintain the saturation temperature (100 °C at 1 atm.). During the actual measurement at certain heat flux, the cartridge heaters where turned off for short period of time and did not therefore influence the movement of liquid in the boiling chamber. The water vapor was converted back to the liquid state in the condenser, placed at the top of the chamber. Two T-type thermocouples were used to measure the water temperature (T_{sat}) and were placed about 0.5 cm under and above the boiling surface, respectively. The metal foil was powered by a Sorensen SGA 40/250 DC power supply and the electrical current was measured indirectly by measuring the voltage drop across the shunt. As the thin metal foil was heated by the Joule effect, the heat flux was calculated as a product of current and voltage drop across the foil divided by its surface area. We assumed a constant heat generation across the entire foil. All of the temperature and voltage signals were recorded with an Agilent 34970A data acquisition unit and a multiplexer module 34901A. The visualization system consisted of high-speed CMOS cameras (Casio Exilim EX-F1 and Vision Research Phantom v4.1) and a high-speed IR camera (FLIC SC6000), all of which recorded at 1000 fps. The average and local wall temperatures (T_w) were obtained from IR images with a spatial resolution of 250 μm.

2.3. Measurement uncertainties

The stainless-steel foils were painted on the bottom with high-emissivity paint to improve the IR thermography. The paint was custom made and consisted of 40% silicone-polyester binder and 60% amorphous carbon (Pigment Black 7). The average spectral emissivity of the paint was measured to be 0.9 in the mid-wave infrared band (3–5 μm). Since the boiling occurs at the top of the foils and we are observing the temperature field at the bottom, we estimated the thermal time constant of each individual layer to be:

$$\tau = \frac{\delta^2 \rho c_p}{k} \tag{1}$$

where δ, ρ, c_p and k represent the layer thickness, density, specific heat, and thermal conductivity, respectively. Considering the material properties, listed in Table 3, the thermal time constants are 47.5 μs, 154 μs, and 9.4 μs for the high-emissivity paint, the stainless-steel foil, and the PDMS-silica coating, respectively. The thermal response of the heater is thus appropriate for the frame rate of the IR camera (1000 fps). It was assumed that the PDMS-silica coating consisted only of PDMS, which has a lower thermal conductivity compared to the amorphous silica thin film [21,22].

The overall wall temperature at certain heat flux was calculated as an average from ten thousand frames (10 s of recording), each representing two-dimensional temperature field. The conversion from raw digitalized IR signal to temperature was calculated via calibration curve, obtained at the same ambient conditions as were later maintained during actual boiling experiments. The absolute measurement uncertainty of the temperature measurement was determined to be around 2 K and was practically constant in the entire calibration range (80–180 °C).

Expanded relative measurement uncertainty of the heat flux was estimated as 0.5% of the heat flux. This resulted from combined measurement uncertainty of the voltage drop across the foil, electrical current and uncertainty of the heater area. The uncertainty of the heat transfer coefficient depends on inaccuracies in heat flux and wall temperature measurements. Maximum uncertainty of the heat transfer coefficient was 3.5 kW/m^{2}K, which can be greater than 100% of the value at low heat fluxes and low superheats. However, relative uncertainty decreases as the superheat and heat flux increase.

3. Results and discussion

3.1. Surface characterization

In order to characterize the boiling surfaces and to understand the wetting transition from hydrophobic to superhydrophilic, analyses using contact-angle measurements, scanning electron microscopy with energy-dispersive X-ray spectroscopy (SEM/EDS), atomic force microscopy (AFM), and Fourier-transform infrared spectroscopy (FTIR) were performed. A detailed list of the measuring equipment is given in Table 1.

3.1.1. Contact angles

The contact-angle measurements that were performed at ambient temperature prior to the boiling experiments revealed that the stainless-steel foil with a static contact angle (θ) of 87.8° becomes highly hydrophobic after the deposition of the PDMS-silica coating. The contact angle was measured to be 137.8°, as shown in Fig. 3. This contact angle is significantly higher than 101° for bulk PDMS [23], which suggest a structured surface. The free-surface energies of the bare and coated foils were 30.9 mJ/m^2 and 2.65 mJ/m^2, respectively. After the laser thermal treatment, the hydrophobic coating becomes superhydrophilic, since the contact angle of the water was found to drop below the limit of the measurement (<1°), as seen in Fig. 3(c). The same transition from hydrophobic to superhydrophilic was observed after annealing the PDMS-silica coated foils for 8 h at 600 °C.

3.1.2. SEM/EDS analysis

The SEM image, shown in Fig. 4(b), reveals that the hydrophobic PDMS–silica coating is textured by randomly distributed micro-cavities and micro-islands. It is clear that during the laser thermal treatment some of the coating material was ablated, resulting in a modified, but still porous, micro-topography. This also partially explains the change in the optical transparency of the coating after the laser treatment [Fig. 4(a)]. Very comparable results can be found in a paper by Schutzius et al. [24], where they studied the wettability transition during the thermal treatment of a methylsilsesquioxane-silica coating. Fig. 4(c) shows that silicon, oxygen and carbon were detected in the hydrophobic PDMS-silica coating. A peak, characteristic of carbon atoms, is due to the presence of methyl groups on the surface and could not result from the stainless-steel substrate, since no other element typical of stainless-steel is detected. It should also be noted that the same EDS spectra can be observed on the very edge of the hydrophobic

Table 3
Material properties of the stainless-steel foil, high-emissivity paint, and PDMS.

Material	Thickness δ (μm)	Density ρ (kg/m^3)	Specific heat c_p (kJ/kgK)	Thermal conductivity k (W/mK)
Stainless steel, S316	25	7990	0.50	16.2
High-emissivity paint	5	1560	0.95	78.0
PDMS [21]	1	970	1.46	0.15

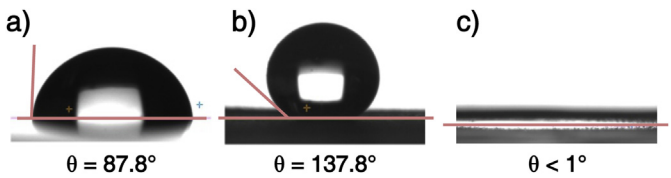

Fig. 3. Contact angles of the water: (a) on the bare stainless-steel foil; (b) on the hydrophobic PDMS-silica coated foil; (c) on the superhydrophilic laser treated surface.

squared spot, indicating a sharp transition between the hydrophobic and superhydrophilic regions [Fig. 4(d)]. Even though the EDS spectra of the superhydrophilic, laser-treated surface show elements that are typical of stainless steel [e.g., see Fig. 4(e)], a layer of the material from the original hydrophobic coating still remains on the surface, since the silicon and oxygen peaks were not detected on the bare, stainless-steel foil, as seen in Fig. 4(f).

3.1.3. AFM microscopy

Fig. 5(b) and (c) shows that the hydrophobic, micro-roughened surface is covered with spherical particles with sizes of 10–50 nm, which correspond to the primary particle size of the fumed silica (10 nm). On the other hand, the surface of the bare stainless-steel foil, shown in Fig. 5(a), is relatively smooth compared to the coated foils. Introducing the hydrophobic silica particles into the coating therefore results in a hierarchical micro- and nano-roughened surface, which was already shown to exhibit highly hydrophobic, or even superhydrophobic, properties [24,25].

The boundary between the hydrophobic coating and the superhydrophilic, laser-treated coating is presented in Fig. 6(a). From Fig. 5(c) and 6(b–c), it is clear that the nano-scaled textures are very comparable, even though the micro-topography is completely changed after the laser treatment. Furthermore, the superhydrophilic, laser-treated coating [Fig. 6(b)] and the superhydrophilic annealed coating [Fig. 6(c)] exhibit very similar nanostructures, with silica particles still present on the surface.

3.1.4. FTIR spectroscopy

The FTIR spectra of the hydrophobic PDMS-silica coating and the superhydrophilic annealed PDMS-silica coating are presented in Fig. 7. The spectrum of the basic hydrophobic coating is typical for the polydimethylsiloxane/silica composite, with peaks indicating the Si–O–Si and Si–CH_3 structures. The peak at 2966 cm^{-1} also indicates the C–H stretching in the –CH_3 groups. After annealing the coating in the furnace for 8 h at 600 °C, the methyl groups are no longer present, due to their oxidation. Instead, the spectrum of the superhydrophilic surface shows peaks indicating silicon dioxide and silicon carbide. Both materials are a result of the thermal degradation of the PDMS. Silicon carbide is more likely to be formed at higher heating rates [27], such as with a laser treatment. However, because the FTIR analysis was not possible on the laser-treated surface, due to the low thickness of the remaining coating, we assume that the laser-treated coating exhibits a similar surface chemistry to the annealed surface.

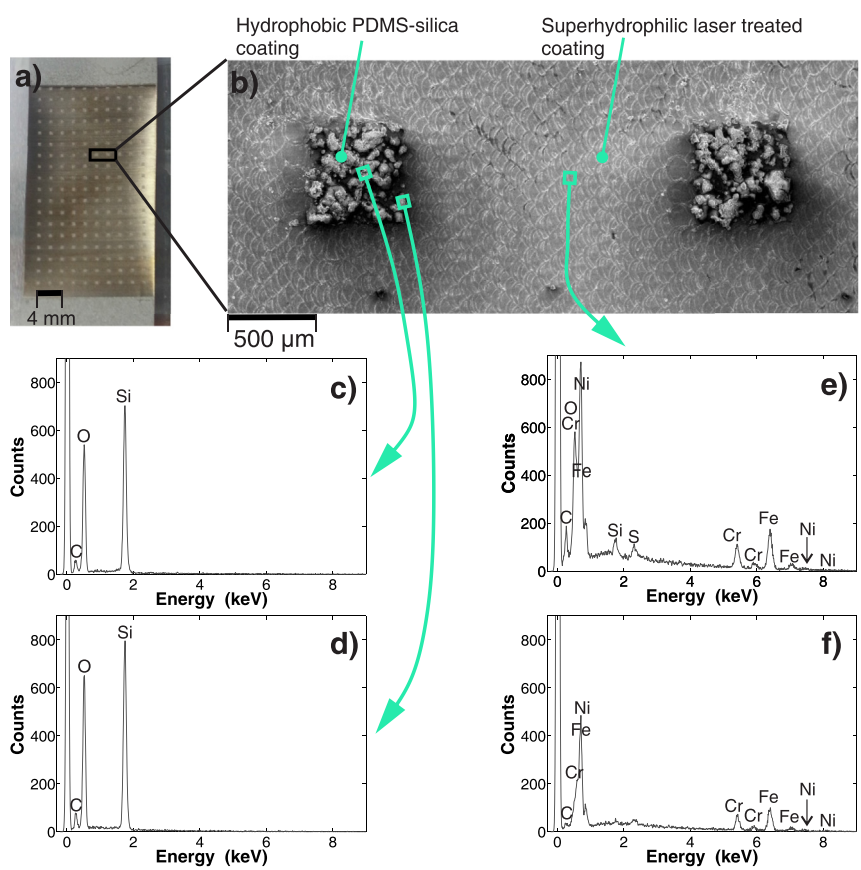

Fig. 4. (a) Photograph and (b) magnified SEM image of the 0.5 × 0.5 mm^2 hydrophobic spot surrounded with the superhydrophilic network; (c)–(d) EDS of the hydrophobic spot; (e) EDS of the laser-treated superhydrophilic surface; (f) EDS of the bare stainless-steel foil.

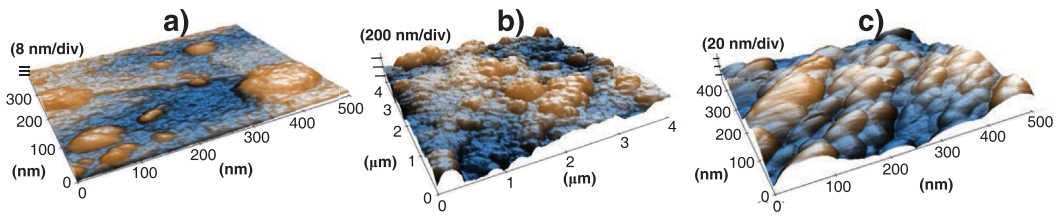

Fig. 5. AFM results: (a) on the bare stainless-steel foil; (b)–(c) on the hydrophobic PDMS-silica coating.

3.2. Nucleate boiling performance on the surfaces with uniform wettability

The boiling curves on the bare, stainless-steel (SS), superhydrophilic (SHPI), and hydrophobic (HPO) surfaces are presented in Fig. 8. For comparison, some boiling performances on state-of-the-art surfaces made on silicon [15,28] and titanium [29] are also shown in Fig. 8. The critical heat flux on the SHPI surface (1402 kW/m^2) was more than 350% of that on the SS surface (301 kW/m^2). Due to the increased roughness and increased wettability, which decreases the contact diameter and therefore the departure diameter of the bubbles, the SHPI surface provides a higher density of nucleation sites. This can be confirmed by comparing the average wall temperature fields during the boiling on the SHPI and SS surfaces, as shown in Fig. 9. An analysis of the temperature fields at 300 kW/m^2 revealed that the average maximum bubble contact diameter on the SS surface was 4 mm and the nucleation-site density was approximately 4 sites/cm, while on the SHPI surface the contact diameters were around 1.3 mm with a nucleation-site density of 16 sites/cm. At the same time, the SHPI surface requires larger superheat for the bubbles to occur, since the minimum average wall temperature at 300 kW/m^2 is around 113.1 °C, and on the SS surface only 107.3 °C. However, the SHPI surface provides a somewhat higher HTC, due to the increased surface roughness (i.e., an increased surface area for the heat transfer) and a higher density of active nucleation sites, compared to the SS surface. We also found that maximum local wall temperature close to CHF was 163 °C on the SHPI surface and 159 °C on the SS surface. These values are very comparable despite the fact that average wall temperature close to CHF was 143 °C on the SHPI surface and only 122 °C on the SS surface. This clearly indicates that increased "suction" of the liquid to the nucleation sites delays the dry-out of the SHPI surface and enhances the CHF [4,12,15,29].

The HPO surface exhibited completely different boiling behavior compared to the SS and SHPI surfaces. The formation of vapor bubbles occurred at the wall superheat of less than 1 K and the wall temperature reached 135.2 °C at only 7.1 kW/m^2. It was hard to observe the nucleate boiling since the vapor film almost instantly covered the entire heating area. However, at small heat fluxes, the HPO surface exhibited a relatively high HTC, which implies that it promotes boiling incipience compared to the other surfaces with uniform wettability. This is in accordance with the results of Takata et al. [30], who made experiments involving the saturated and subcooled boiling of water on a superhydrophobic ($\theta = 152°$) surface. The formation of a vapor film could be due to the remaining gas, trapped in the cavities of the HPO surface, that prevents the fluid from completely wetting the cavities because of the capillary pressure, as found by Wang et al. [31].

3.3. Nucleate boiling performance on biphilic surfaces

Fig. 10 shows the heat flux as a function of the superheat and the HTC as a function of the heat flux for biphilic (BPI) surfaces. It is clear, that all the BPI surfaces exhibit a steeper boiling curve than the surfaces with uniform wettability, with the CHF values being in the range from 700 kW/m^2 to 900 kW/m^2, which is up to 200% of that on a bare SS surface. We achieved the highest measured HTC (51.2 kW/m^2) on the $BPI_{0.25}$. On average, all the BPI surfaces provided an approximately 61% enhancement in the HTC compared to the SHPI surface. However, none of the BPI surfaces exhibited a higher CHF than the SHPI surface. Compared to the biphilic surfaces that were investigated by other authors [14,15], ours provided a higher HTC, but exhibited a much

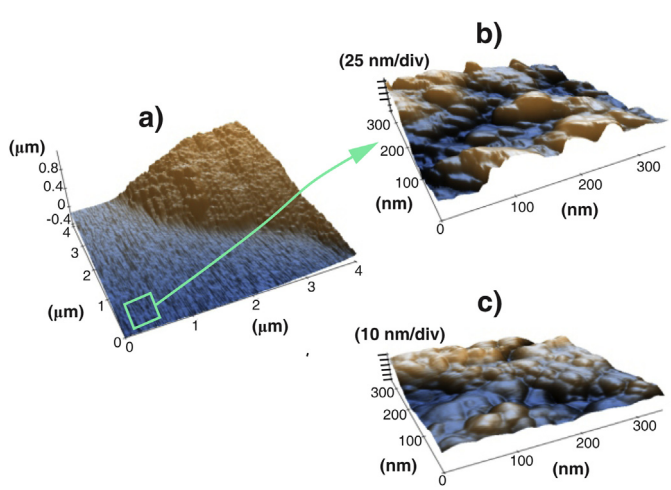

Fig. 6. AFM results: (a) on the transition between the superhydrophilic, laser-treated coating and the hydrophobic squared spot; (b) magnified view of the superhydrophilic laser-treated coating; (c) on the superhydrophilic annealed coating.

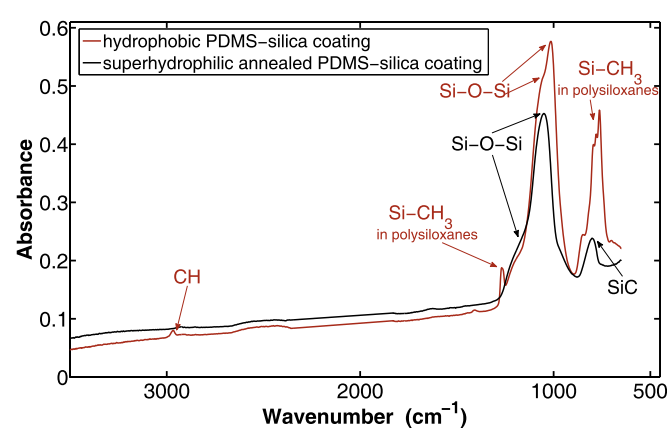

Fig. 7. FTIR spectra for the hydrophobic PDMS-silica coating and the superhydrophilic annealed PDMS-silica coating, with the arrows indicating the peaks [26] of interest.

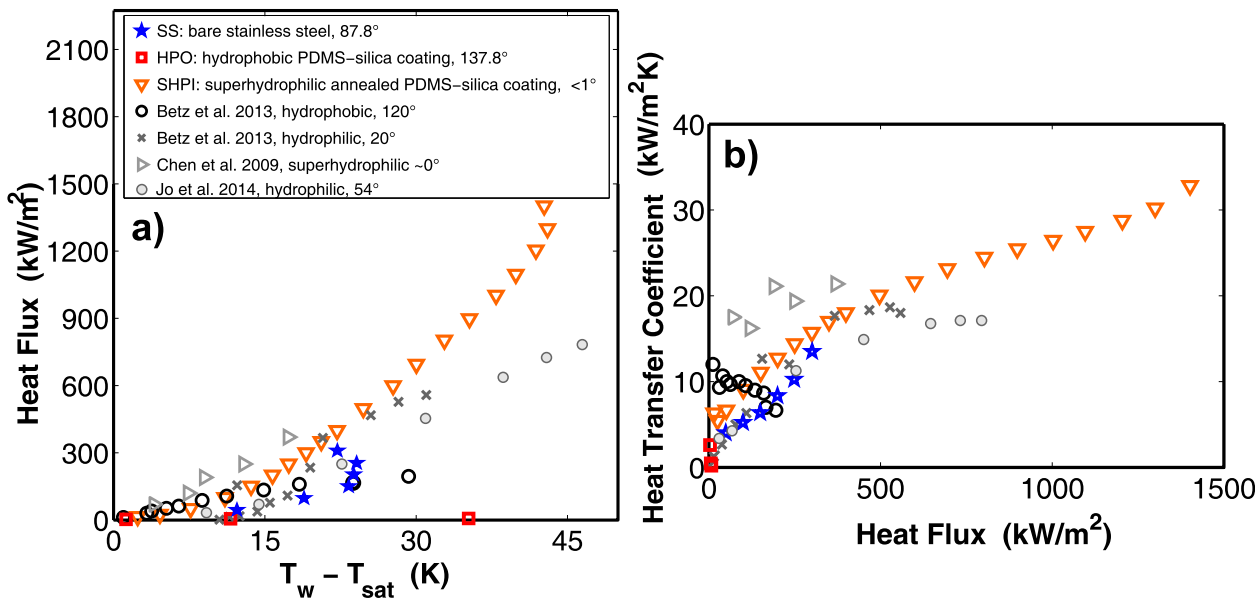

Fig. 8. (a) Heat flux vs. superheat and (b) HTC vs. heat flux for surfaces with a uniform wettability. Some recently published results of pool boiling of water on hydrophobic, hydrophilic [15,28], and superhydrophilic [29] surfaces are also shown.

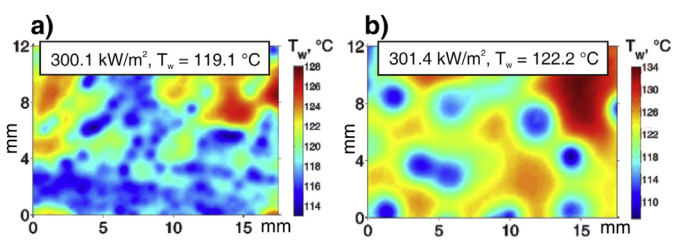

Fig. 9. An average temperature field of 10000 frames during nucleate boiling (a) on the superhydrophilic surface and (b) on the bare, stainless-steel foil close to the CHF at approximately 300 kW/m^2.

inferior boiling performance in comparison with the superbiphilic surface [15]. It must be noted that Betz et al. [15] used a surface with 40-μm superhydrophobic spots and a pitch of 100 μm, surrounded by a superhydrophilic network. These dimensions are almost one order of magnitude smaller than those on our $BPI_{0.25}$ surface. This demonstrates the importance of the high wettability contrast and the pattern dimensions to the boiling performance.

Fig. 11, showing typical video frames of pool boiling, confirms that the patterns of the hydrophobic spots, surrounded by the hydrophilic network, provide active nucleation sites. Moreover, it also shows that smaller spots reduce the bubble diameter. The average bubble departure diameters were 0.9 mm and 1.7 mm on the $BPI_{0.25}$ and BPI_2 surfaces, respectively. Consequently, at 25 kW/m^2 the average nucleation frequency was measured to be 85 Hz on the

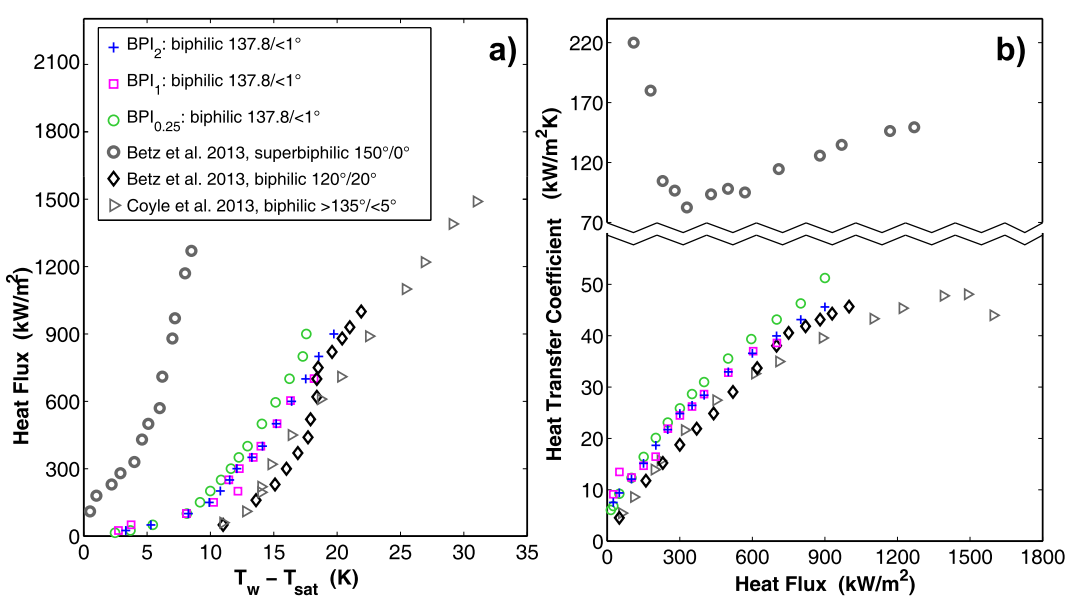

Fig. 10. (a) Heat flux vs. superheat and (b) HTC vs. heat flux for biphilic surfaces. For a better comparison with our results, some recently published results of pool boiling of water on biphilic [14,15] surfaces are also shown.

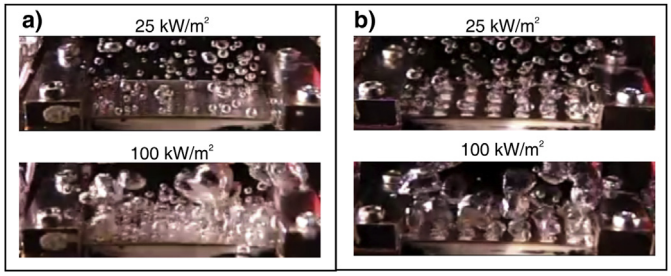

Fig. 11. Sample video frames of pool boiling (a) on the $BPI_{0.25}$ and (b) on the BPI_2 surface for the 25 kW/m^2 and 100 kW/m^2.

$BPI_{0.25}$ surface and only 43 Hz on the BPI_2 surface, which is consistent with Malenkov's correlation [32]. Furthermore, the superhydrophilic region prevents the bubble coalescence on the heater surface and thus allows the bulk water to be supplied to the nucleation sites, as is clearly presented in Fig. 11(b).

Fig. 12 presents the average temperature fields of 10,000 fames (the left-hand-side image) at different heat fluxes and wall-temperature variations (the right-hand-side image) over a selected time span on a single 2-mm hydrophobic spot (marked with rectangle 2) and the neighboring superhydrophilic region (marked with rectangle 1). At 100 kW/m^2, the hydrophobic spots exhibit lower temperatures, indicating that the boiling takes place on those sites, especially on the borders between the hydrophobic and the superhydrophilic regions, as presented in Fig 12(a). This boiling on the borders was also observed by other authors [13,31] and it is most likely due to the relatively low thermal conductivity of the PDMS (0.15 W/mK). For comparison, the thermal conductivity of the stainless steel is 16.2 W/mK and the border regions may therefore experience higher temperatures than the central regions of the hydrophobic spots. At 300 kW/m^2, the average temperature of the hydrophobic spot rises above the temperature of the surrounding superhydrophilic network. At this point, the hydrophobic spot is almost completely covered by a vapor, allowing us to locally observe the film boiling regime. Even though the bubbles still arise from hydrophobic spots, the temperature remains relatively constant [e.g., see the right-hand side of Fig. 12(b)]. This further confirms the existence of the vapor film. Due to the reduced HTC on the hydrophobic spots, the bubbles start to form on the superhydrophilic region and exhibit similar behavior as on the pure SHPI surface. We should also note that the BPI_1 surface exhibited similar boiling performance to the BPI_2 surface.

During boiling on the $BPI_{0.25}$ surface, the hydrophobic spots represent active nucleation sites and exhibit lower temperatures than the surrounding superhydrophilic network, as is clear from Fig. 13. The temperature fluctuations at the selected hydrophobic spot demonstrate the vigorous boiling that also affects the temperature variations of the surrounding superhydrophilic region. At a high heat flux [e.g., see Fig. 13(c)] elongated patches of a lower temperature imply that the nearby bubbles start to coalesce. At some point, those coalescences may cause the local dry-out, leading to the burnout of the foil.

The $BPI_{0.25}$ surface provides a higher density of active nucleation sites compared to the BPI_2. Smaller hydrophobic spots also prevent the occurrence of a vapor film, which we observed on the 2-mm spots. Consequently, the $BPI_{0.25}$ surface exhibits, on average, a 10% higher HTC compared to the BPI_2. Above results implies that for a

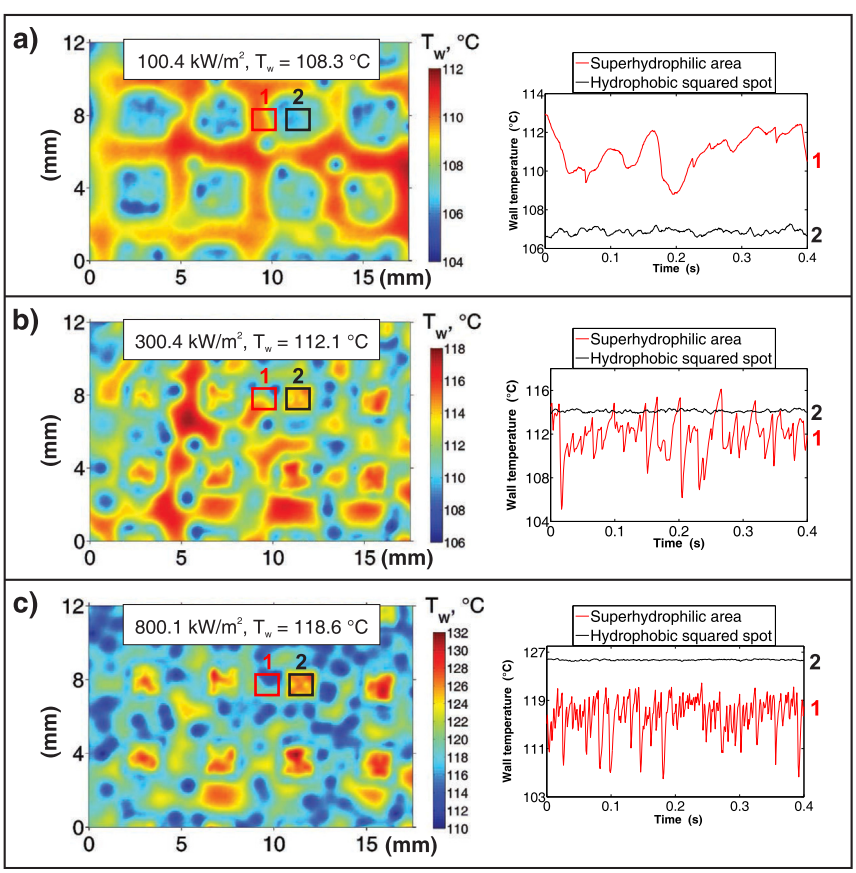

Fig. 12. Average wall temperatures (the left-hand-side image) at (a) 100 kW/m^2, (b) 300 kW/m^2, and (c) 800 kW/m^2 during pool boiling on the BPI_2 surface. The corresponding temperature variations at a selected hydrophobic spot and the surrounding superhydrophilic region are shown on the right-hand side of the image.

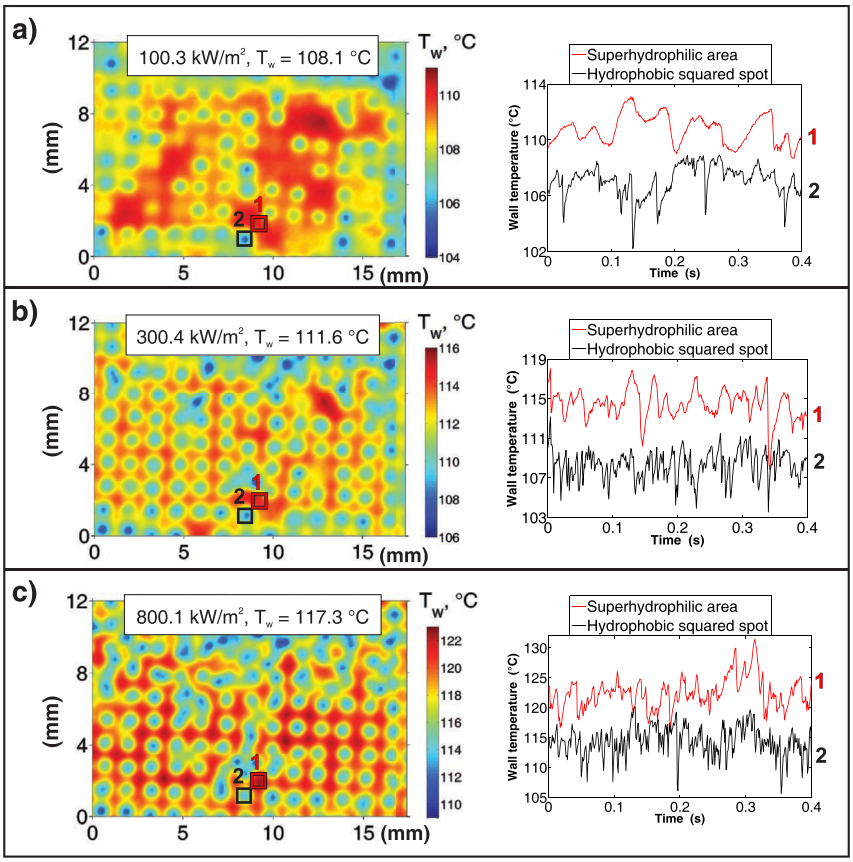

Fig. 13. Average wall temperatures (the left-hand-side image) at (a) 100 kW/m^2, (b) 300 kW/m^2, and (c) 800 kW/m^2 during pool boiling on the $BPI_{0.25}$ surface. The corresponding temperature variations at a selected hydrophobic spot and the surrounding superhydrophilic region are shown on the right-hand side of the image.

certain heat flux, there must exist some minimum superhydrophilic region between two hydrophobic spots, which will prevent bubble coalescence and thus form two separate nucleation sites. At the same time, one can ask a maximum size of the hydrophobic spot, above which the vapor film would not form. Finding those two limits could help further increase the HTC on a biphilic surfaces. However, the improvement in the CHF is questionable, since the highest CHF was achieved on a completely superhydrophilic surface.

4. Conclusions

This study presents boiling heat transfer enhancement on superhydrophilic and micro-patterned hydrophobic/superhydrophilic surfaces. Thin, stainless-steel foils were air-sprayed with the basic coating, made of hydrophobic fumed silica and polydimethylsiloxane resin. Surface analyses showed that the coating exhibits a high hydrophobicity due to its hierarchical structure together with the use of hydrophobic polymer. An appropriate thermal treatment causes the oxidation of methyl groups and the formation of silicon oxide and silicon carbide that result in a wettability transfer from hydrophobic to superhydrophilic. On this basis, the original coating was locally thermal treated with a pulsed Nd:YAG laser to produce biphilic patterns. These so-prepared surfaces have several advantages: (i) straightforward production, (ii) the possibility of covering large areas, and (iii) thermal and mechanical stability to withstand the nucleate pool-boiling process.

The uniform superhydrophilic surface exhibited the highest CHF that was more than 350% of that on a bare, stainless-steel surface. High-speed IR thermography revealed that the increased wettability reduces the bubble contact diameter, allows a higher density of active nucleation sites, as well as delaying the dry-out. The opposite performance was observed on a uniform hydrophobic surface where the vapor film covered the entire heating surface almost immediately after the boiling incipience. However, a hydrophobic surface can provide a high HTC for small heat fluxes, since the first bubble appeared on the surface at a superheat of less than 1 K.

Biphilic surfaces with differently sized hydrophobic spots (2×2 mm^2, 1×1 mm^2 and 250×250 μm^2) exhibited an up to 200% higher CHF compared to the bare stainless steel. Among all the tested surfaces, the highest HTC (51.2 kW/m^2) was achieved on the surface with the smallest hydrophobic spots. We showed that a smaller hydrophobic spot reduces the bubble diameter and increases the nucleation frequency. On the other hand, the surfaces with a larger hydrophobic region promote boiling incipience and therefore exhibit somewhat higher HTCs at low heat fluxes. However, with increasing heat flux, the vapor film starts to cover the hydrophobic regions, creating local dry-outs and reducing the heat transfer. To optimize the biphilic pattern and hydrophobic spot size in order to achieve the best boiling performance, further investigations are needed.

Acknowledgements

Authors would like to thank the Slovenian Research Agency (Research Program: P2-0223) for supporting this study.

References

[1] C. Lee, H. Kim, H.S. Ahn, M.H. Kim, J. Kim, Micro/nanostructure evolution of zircaloy surface using anodization technique: application to nuclear fuel cladding modification, Appl. Surf. Sci. 258 (2012) 8724–8731.
[2] I.C. Bang, J. Buongiorno, L.-W. Hu, H. Wang, Measurement of key pool boiling parameters in nanofluids for nuclear applications, J. Power Energy Syst. 2 (2008) 340–351.
[3] S. Launay, A. Fedorov, Y. Joshi, Hybrid micro-nano structured thermal interfaces for pool boiling heat transfer enhancement, Microelectron. J. 37 (2006) 1158–1164.
[4] Z. Yao, Y.-W. Lu, S.G. Kandlikar, Effects of nanowire height on pool boiling performance of water on silicon chips, Int. J. Therm. Sci. 50 (2011) 2084–2090.
[5] A.D. Reeser, Energy Efficient Two-phase Cooling for Concentrated Photovoltaic Arrays, Department of Mechanical Engineering, Vol. Master of Science, University of Maryland, Faculty of the Graduate School, College Park, 2013, p. 106.
[6] Y.-W. Lu, S.G. Kandlikar, Nanoscale surface modification techniques for pool boiling enhancement - a critical review and future directions, in: 8th Int. Conf. on Nanochannels, Microchannels, and Minichannels, ASME, Montreal, 2010, pp. 1–12.
[7] M.S. El-Genk, A.F. Ali, Enhanced nucleate boiling on copper micro-porous surfaces, Int. J. Multiph. Flow 36 (2010) 780–792.
[8] S. Vemuri, K.J. Kim, Pool boiling of saturated FC-72 on nano-porous surface, Int. Commun. Heat Mass Transf. 32 (2005) 27–31.
[9] K.-H. Chu, R. Enright, E.N. Wang, Structured surfaces for enhanced pool boiling heat transfer, Appl. Phys. Lett. 100 (2012), 241603 241601–241604.
[10] Z.G. Xu, C.Y. Zhao, Thickness effect on pool boiling heat transfer of trapezoid-shaped copper foam fins, Appl. Therm. Eng. 60 (2013) 359–370.
[11] S. Ujereh, T. Fisher, I. Mudawar, Effects of carbon nanotube arrays on nucleate pool boiling, Int. J. Heat Mass Transf. 50 (2007) 4023–4038.
[12] B. Shi, Y.-B. Wang, K. Chen, Pool boiling heat transfer enhancement with copper nanowire arrays, Appl. Therm. Eng. 75 (2015) 115–121.
[13] A.R. Betz, J. Xu, H. Qiu, D. Attinger, Do surfaces with mixed hydrophilic and hydrophobic areas enhance pool boiling? Appl. Phys. Lett. 97 (2010).
[14] C. Coyle, H. O'Hanley, B. Phillips, J. Buongiorno, T. McKrell, Effects of hydrophobic surface patterning on boiling heat transfer and critical heat flux of water at atmospheric pressure, in: ASME 2013 Power Conference, Masschusetts, 2013, pp. 1–6.
[15] A.R. Betz, J. Jenkins, C.-J. Kim, D. Attinger, Boiling heat transfer on superhydrophilic, superhydrophobic, and superbiphilic surfaces, Int. J. Heat Mass Transf. 57 (2013) 733–741.
[16] R. Bertossi, N. Caney, J.A. Gruss, O. Poncelet, Pool boiling enhancement using switchable polymers coating, Appl. Therm. Eng. 77 (2015) 121–126.
[17] Z.G. Xu, C.Y. Zhao, Influences of nanoparticles on pool boiling heat transfer in porous metals, Appl. Therm. Eng. 65 (2014) 34–41.
[18] Y. Tang, B. Tang, Q. Li, J. Qing, L. Lu, K. Chen, Pool-boiling enhancement by novel metallic nanoporous surface, Exp. Therm. Fluid Sci. 44 (2013) 194–198.
[19] L. Dong, X. Quan, P. Cheng, An experimental investigation of enhanced pool boiling heat transfer from surfaces with micro/nano-structures, Int. J. Heat Mass Transf. 71 (2014) 189–196.
[20] Y. Takata, S. Hidaka, T. Uraguchi, Boiling feature on a super water-repellent surface, Heat. Transf. Eng. 27 (2006) 25–30.
[21] Polymer Data Handbook, Oxford University Press, Oxford, 1999.
[22] S.-J. Moon, H. Jung, Estimation of thermal conductivity of amorphous silicon thin films from the optical reflectivity measurement, J. Nanosci. Nanotechnol. 13 (2013) 6362–6366.
[23] M.J. Owen, in: J.E. Mark (Ed.), Physiscal Properties of Polymers Handbook, AIP Press, New York, 1996, p. 669.
[24] T.M. Schutzius, I.S. Bayer, G.M. Jursich, A. Das, C.M. Megaridis, Superhydrophobic-superhydrophilic binary micropatterns by localized thermal treatment of polyhedral oligomeric silsesquioxane (POSS)-silica, Nanoscale 4 (2012) 5378–5385.
[25] C.R. Crick, I.P. Parkin, Preparation and characterisation of super-hydrophobic surfaces, Chem. A Eur. J. 16 (2010) 3568–3588.
[26] A.L. Smith, Infrared spectra-structure correlations for organosilicon compounds, Spectrochim. Acta 16 (1960) 87–105.
[27] G. Camino, S. Lomakin, M. Lazzari, Polydimethylsiloxane thermal degradation part 1. Kinetic aspects, Polymer 42 (2001), 2935–2402.
[28] H. Jo, S. Kim, H.S. Park, M.H. Kim, Critical heat flux and nucleate boiling on several heterogeneous wetting surfaces: controlled hydrophobic patterns on a hydrophilic substrate, Int. J. Multiph. Flow 62 (2014) 101–109.
[29] Y. Chen, D. Mo, H. Zhao, N. Ding, S. Lu, Pool boiling on the superhydrophilic surface with TiO2 nanotube arrays, Sci. China Ser. E Technol. Sci. 52 (2009) 1596–1600.
[30] Y. Takata, S. Hidaka, J.M. Cao, T. Nakamura, H. Yamamoto, M. Masuda, T. Ito, Effect of surface wettability on boiling and evaporation, Energy Fuels 30 (2005) 209–220.
[31] X. Wang, S. Zhao, H. Wang, T. Pan, Bubble formation on superhydrophobic-micropatterned copper surfaces, Appl. Therm. Eng. 35 (2012) 112–119.
[32] I.G. Malenkov, Detachment frequency as a function of size for vapor bubbles, J. Eng. Phys. 20 (1971) 704–708.